1997 HST Calibration Workshop
Space Telescope Science Institute, 1997
S. Casertano, et al., eds.

NICMOS PSF Variations and Tiny Tim Simulations

John E. Krist

Space Telescope Science Institute, 3700 San Martin Drive, Baltimore, MD 21218, USA

Richard N. Hook

Space Telescope – European Coordinating Facility, European Southern Observatory, Karl Schwarzschild Str. 2, D-85748, Garching, Germany

Abstract. Analysis of NICMOS images indicates that the instrument's optics provide high quality imaging over the wavelength range and field of view of the cameras (assuming that NICMOS 3 can be placed in-focus during campaign modes). Optical misalignments and low-level field- and focus-dependent aberrations have slight effects on the imaging performance. Variations of the point-spread functions (PSFs) with wavelength may be important when comparing images through different filters, especially in NICMOS 1 due to its high resolution.

The NICMOS 1 and 2 camera cold masks are shifted with respect to the telescope obscurations, causing elliptical diffraction rings and alteration of the diffraction spike patterns. The mask shift varies with time, altering the diffraction structure mostly in the wings and spiders. It is not currently known whether the NICMOS 3 mask is similarly shifted.

The effects of these alignment and optical surface errors can be studied using the Tiny Tim PSF modeling software. The NICMOS field and focus dependent aberrations and obscuration misalignments derived from the image measurements are included in the simulated PSFs, along with variations due to the filter passbands. The model PSFs match the observed ones well.

1. Introduction

When dealing with images from the Hubble Space Telescope (HST) it is necessary to be aware of the characteristics of the point spread function (PSF). The PSF often defines the resolution and sensitivity limits of an observation, rather than the sizes or efficiencies of the detector pixels. Unfortunately, the PSF can vary with time, wavelength, position, and camera. Because of the wavelengths at which it operates, NICMOS has PSFs which differ markedly from those in the other HST cameras (WFPC2, FOC).

NICMOS PSFs vary from well sampled (NICMOS 1 at long wavelengths) to significantly undersampled (NICMOS 3 at shorter wavelengths). One must deal with the large size of the diffraction structure at long wavelengths, which effectively limits the object resolution in some cases. In NICMOS 2, shifting obscurations cause spider patterns and diffraction rings in the wings to vary with time. These changes may be larger than those caused by breathing or object color effects.

These effects can be well modeled by Tiny Tim, a program which can generate simulated PSFs for any wavelength or filter. Tiny Tim PSFs are good matches to the observed ones, making them useful for photometry, deconvolution, and image modeling.

Note: In the following discussions, we assume that NICMOS 3 is in-focus, as it will be during observing campaigns with the HST secondary mirror adjusted.

2. Wavelength Variations

PSF diffraction structures (Airy rings, spiders) grow larger with increasing wavelength. At longer wavelengths the detector pixels better sample the PSF. This has consequences with regards to sensitivity and contrast.

For instance, as shown in Table 1, in NICMOS 1 (f/80, 0.043" pixels) at 2.2μm the peak pixel contains only 3% of the total flux, and the PSF core has a FWHM of over four pixels. The first Airy ring is about 15 pixels (0.65") in diameter. In this case a significant amount of light is distributed over a number of pixels. At 1.1μm the FWHM is 2.3 pixels (0.1") with 10% of the total flux in the central pixel. In NICMOS 2 (f/45, 0.076" pixels) the situation is less drastic, since that camera undersamples the PSF at wavelengths less than 1.8μm. The large pixels of NICMOS 3 (f/17.2, 0.2" pixels) result in the FWHM remaining constant in that camera, as it undersamples over the entire NICMOS wavelength range.

Table 1. PSF Widths and Peak Pixel Fluxes

	1.1μm FWHM (pixels)	1.1μm Flux in Peak	2.2μm FWHM (pixels)	2.2μm Flux in Peak
NICMOS 1	2.3 (0.1")	10%	4.5 (0.2")	3%
NICMOS 2	1.3 (0.1")	25%	2.5 (0.2")	8%
NICMOS 3	1.3 (0.3")	52%	1.3 (0.3")	39%

One must be cautious when comparing images at different wavelengths taken in NICMOS 1, and to a lesser degree in NICMOS 2. Objects with sharp features may show color differences between PSFs rather than actual spatial color gradients. Also, the measures of object widths are limited to the PSF width at a given wavelength (jet widths or nebula tendrils, for instance). It is especially important to convolve data models with a PSF before comparing with observed images. An example of this is shown in Figure 1.

Because little light is in the peak pixel at long wavelengths in NICMOS 1 and 2, deconvolution may provide improvements in sharpness. As discussed later, Tiny Tim model PSFs match the observed ones well and have the advantage that they are noiseless. However, as Figure 1 demonstrates, deconvolution may introduce image artifacts which can negate its advantages.

Narrow-band filter images will show very sharp diffraction structures, since the PSF does not vary significantly over the filter bandpass. A PSF in a wide-band filter is smoother, since the expansion of the diffraction structure over the filter's wavelength range blurs the rings. Figure 2 shows observed and model NICMOS 2 PSFs in different filters.

The PSFs in wide-band (and to a lesser degree, medium-band) filters are somewhat dependent on the spectrum of the object being observed. Within the same filter, the PSF of a very red object will be slightly different from that of a blue one. In most cases, the differences will actually be insignificant (except, for example, if one is comparing well-exposed PSFs of M versus O type stars). See the discussion on PSF subtraction by Krist (1997) in these proceedings.

Another aspect of increasing wavelength is that the PSF becomes less sensitive to aberrations in the system, as the path length differences caused by optical surface errors become smaller relative to the wavelength of the light. One-quarter of a wave of an aberration at $\lambda = 0.5\mu$m is only 1/16 wave at $\lambda = 2\mu$m.

3. Field and Focus Dependent Aberrations

As with any real-world optical system, NICMOS has low level aberrations which cause observed PSFs to differ slightly from theoretically perfect ones. The dominant aberrations

Figure 1. A simulation of Io on NICMOS 1 (0.043"/pixel), assuming that Io appears constant with wavelength. All images are at the same angular scale, which is indicated in the upper right image. The mapping of the image onto NICMOS 1 detector pixels is shown at the top, without the PSF. In the lower left frame, the image has been convolved with a 1μm PSF, and by a 2μm PSF to its right. Note that the differences in light distribution between the two. The 2μm deconvolved image reveals artifacts of the restoration process, notably brightening of the left limb.

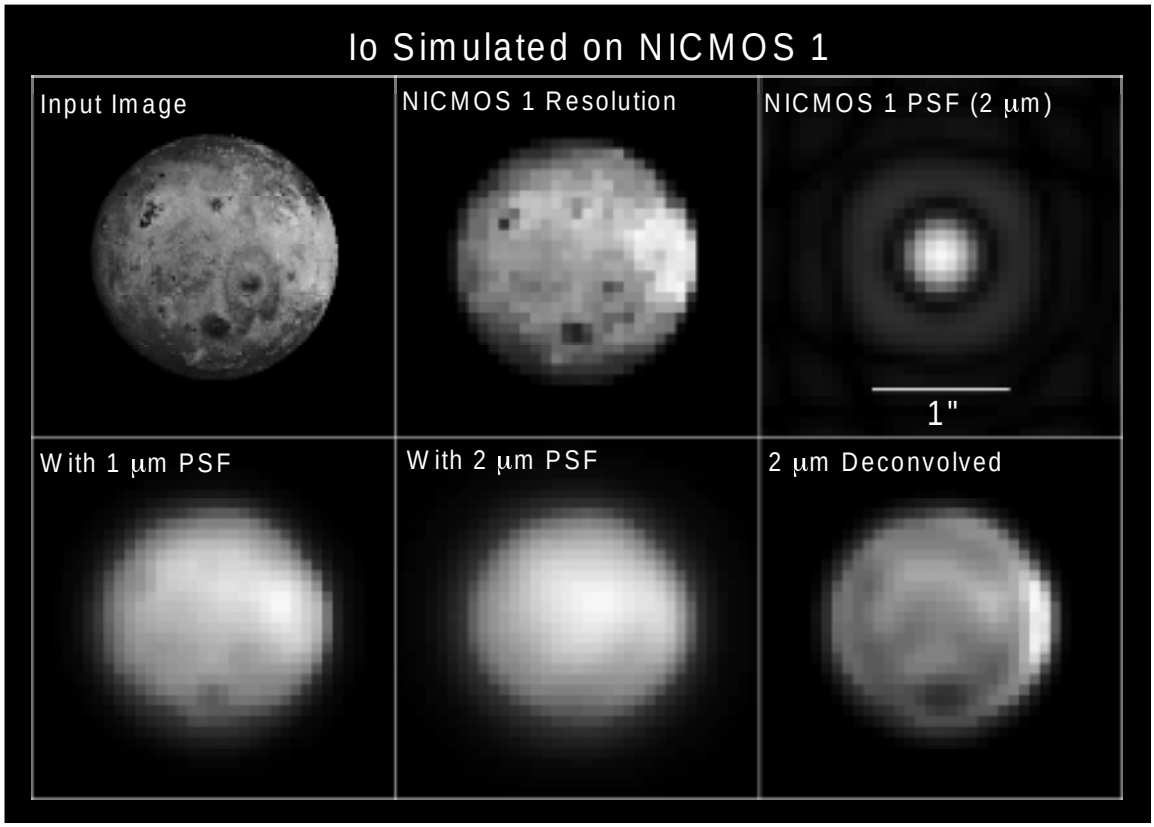

Figure 2. Variations of the NICMOS 2 PSF with wavelength and filter bandwidth. The corresponding Tiny Tim model PSFs are also shown. The images are 10" on a side.

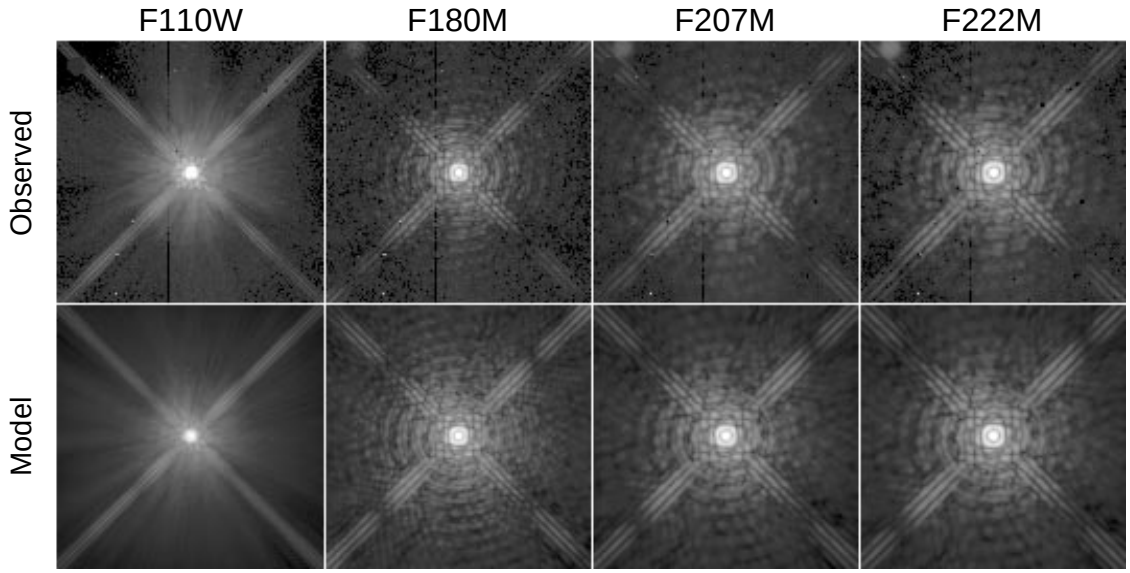

(excluding focus) are coma, astigmatism, and residual spherical aberration. An extensive analysis of NICMOS star images was done using phase retrieval methods (Krist and Burrows 1995) to measure these aberrations and determine their dependence on field position and focus. This used focus monitoring images of a star cluster in which the focus was varied by moving the Pupil Alignment Mechanism (PAM) (phase retrieval is more accurate when defocused PSFs are used).

There is roughly 1/15 of a wave (@ 630 nm) of astigmatism, 1/15 wave of coma, and 1/30 wave of spherical in NICMOS, with the values varying slightly among the three cameras. Some of the astigmatism is due to the imperfect HST optics rather than the camera. The sign and amount of spherical aberration is consistent with that measured in the other corrected HST cameras (WFPC2 & COSTAR/FOC), indicating that the officially designated amount of HST primary mirror spherical aberration is probably in error by a small amount (see Krist & Burrows 1995). In any case these aberrations are small and are similar to those measured in other HST instruments.

Focus, astigmatism, and coma vary slightly with field position, as they do in most optical systems, including WFPC2. The largest variations are in NICMOS 3, due to its larger field of view. The focus in NICMOS 1 and 2 changes linearly with field position, and in NICMOS 3 it varies quadratically with the best focus near the center of the detector. Analysis by Eddie Bergeron (STScI) of the horizontal and vertical plate scales indicates that the detectors are not significantly tilted, so the focus position dependence is due to optical errors or misalignment. Bergeron has also confirmed the focus variations (at least in NICMOS 2) by measuring changes in encircled energy curves. Anatoly Suchkov (STScI) has verified these variations using the same phase retrieval software on later focus monitoring data.

When NICMOS 3 is placed in focus during the upcoming campaigns by moving the telescope's secondary mirror, it will be necessary to adjust the Field Offset Mechanism (FOM) to avoid vignetting. This will introduce changes in the aberrations (mostly astigmatism). The FOM can also be moved during observations with the other cameras to select adjacent fields. The PSFs in those cases will change as well due to increased astigmatism.

Because NICMOS operates at longer wavelengths than the other HST instruments it is less sensitive to aberrations, and they cause little variation on the PSF structure or light distribution. For example, PSFs were simulated using Tiny Tim at 1.6μm at opposite corners of the field of view, with field dependent aberrations included. The variations in flux within small apertures centered on the PSFs were then computed, as shown in Table 2. Because NICMOS 3 undersamples the PSF, it is largely insensitive to small aberration changes.

Table 2. Flux variations between extreme NICMOS field positions

	Aperture Radius (pixels)		
	1	3	5
NICMOS 1	2.2%	1.9%	1.5%
NICMOS 2	3.6%	1.9%	0.7%
NICMOS 3	2.4%	0.0%	0.0%

Coma, astigmatism, and spherical aberration also vary with large changes in focus. However, since the focus of each camera remains essentially constant, the effects on PSFs are negligible. Variations at the level of breathing are not measureable.

4. Cold Mask Misalignment

At the entrance of the dewar containing the NICMOS detectors is a mask intended to block infrared emission from the telescope spiders and primary mirror edge. The mask itself is cooled, hence it is called a cold mask. Each camera has a mask, and those for NICMOS 2 and 3 contain additional tabs to cover the support pads on the HST primary mirror. In NICMOS 2 the mask also serves to reduce scattered light from the telescope obscurations as part of the coronagraph.

The masks and the telescope's obscurations are supposed to be aligned, but recent analysis of NICMOS 2 SNAP images (see Krist (1997) in these proceedings) indicate that camera's mask is shifted with respect to the HST obscurations. The visible results of this shift are elliptical diffraction rings and changes in the banding patterns in the spiders. There are more bands in one spider diagonal than the other, which suggests that the HST and cold mask spiders appear separated along one direction.

Experiments with shifting the NICMOS 2 cold mask in Tiny Tim reproduced these effects well. The mask is shifted by about 11% of the pupil radius (defined by the edge of the telescope primary), with the HST and mask spiders well separated along one direction, as shown in Figure 3. Figure 4 illustrates the difference between PSFs with aligned and shifted masks and the ability of Tiny Tim models to reproduce the effects.

The match between model and observed PSFs is somewhat indirect evidence of the mask shift, but there is more direct proof. Gerchberg-Saxton (GS) phase retrieval can be used to obtain pupil and wavefront information by iteratively solving for the complex-valued optical transfer function (Krist & Burrows 1995). An initial guess for the wavefront and obscuration pattern is provided to the algorithm, and constraints on the pupil function can be enforced at each iteration (such as zero transmission outside of the pupil).

GS algorithms require high signal-to-noise data over a large number of pixels to define the high frequency structure in the pupil function. This typically means that highly defocused PSFs are used, since they have a large number of pixels with similar intensities. In-focus PSFs are usually well exposed in the core but have faint wings, where most of the optical information lies. However, because the SNAP program PSFs are so highly exposed, there is enough signal in the wings to use GS phase retrieval methods.

Figure 3. Simulated obscuration patterns for HST and NICMOS. On the left is the telescope pattern with secondary mirror obscuration, spiders, and mirror support pads. The middle image shows the NICMOS 2 cold mask, which would optimally be aligned with the telescope obscurations. On the right is the predicted NICMOS 2 obscuration pattern with the cold mask shifted. The telescope obscurations are color coded grey.

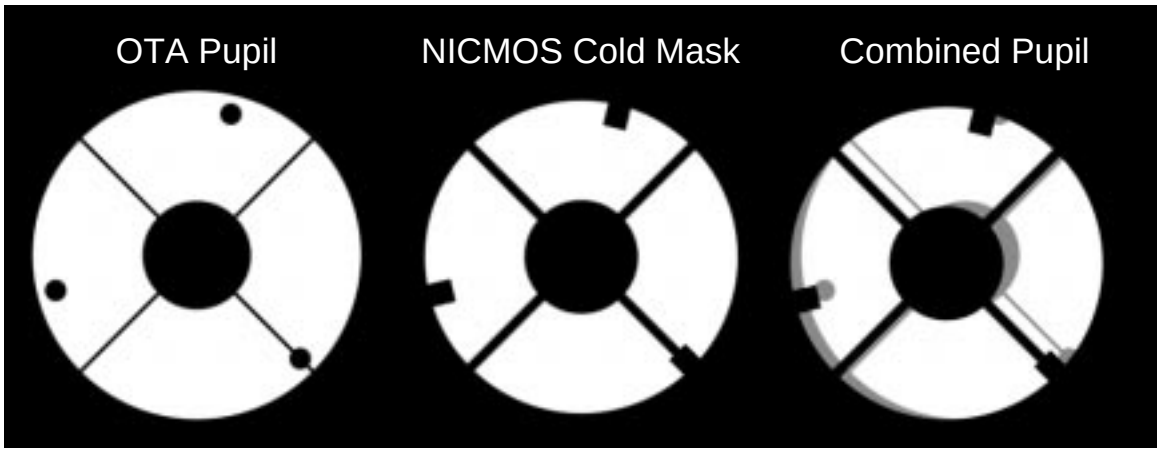

A SNAP PSF was selected which was well exposed and had no companions. The core was saturated, so those pixels were replaced by ones from an unsaturated PSF with a similar registration. GS phase retrieval was applied with only a clear aperture as the initial pupil function. At each iteration the pupil function was constrained to have zero flux outside of it, but no constraints were placed inside.

As shown in Figure 5, at the first iteration the algorithm produced an elliptical central obscuration. In later iterations, as higher frequency structure was fitted, the spider obscurations became more pronounced. Because the telescope pupil is generally symmetrical, there is some amiguity as to which side the mask is shifted - either way would produce most of the same effects in the PSF. Because of this, the GS routine has essentially created two pupils, with the mask shifted to either side of the center. Each pattern contributes half of the throughput of the pupil function. This creates spiders on each side of the thinner telescope spiders along one diagonal, as well as two alternative central obscurations. The offset of the darker (cold mask) spiders from the thinner (telescope) spiders is the same as that derived from the Tiny Tim model experiments.

The shifted mask causes a 10% decrease in throughput relative to an aligned one and reduces the peak pixel by 10% with respect to the total PSF flux. It also likely reduces the efficacy of the coronagraph, since the HST obscurations are not covered. One unsolved problem is how the unmasked portions of the relatively warm HST optics (especially the region outside the primary mirror) contribute to the dark count rate in NICMOS 2. The off-primary region comprises 3% of the clear aperture. There have been no indications of an abnormally high rate, which one would expect with the observed mask shift.

The NICMOS 2 mask appears to shift slightly (0.5% of the pupil radius) and randomly with time (on order of an orbit) about the general offset position. The bands in the spiders change location, with bands along one diagonal moving outwards while those on the other diagonal move inwards. This can only be explained by obscuration shifting, as color or focus variations would cause the bands to move together, and such variations are too small to account for the amount of band motion. There are also small changes in the flux distribution among the rings and core. For example, at $\lambda = 1.6\mu$m, a 0.5% mask shift will change the peak pixel value by 1.1%. In comparison, 3μm of breathing with change the pixel by 0.6%

Figure 4. Examples of the effects of cold mask shift on NICMOS 2 PSFs at 2.2μm. An observed PSF from the NICMOS SNAP program is shown in the upper left. To its right is a Tiny Tim model PSF with the measured aberrations but no mask shift, and a model PSF with mask shift on the right. Notice the circular rings in the aligned mask case, compared to the observed PSF and shifted mask model. Also, the bands in the spiders match between the observed and shifted mask model.

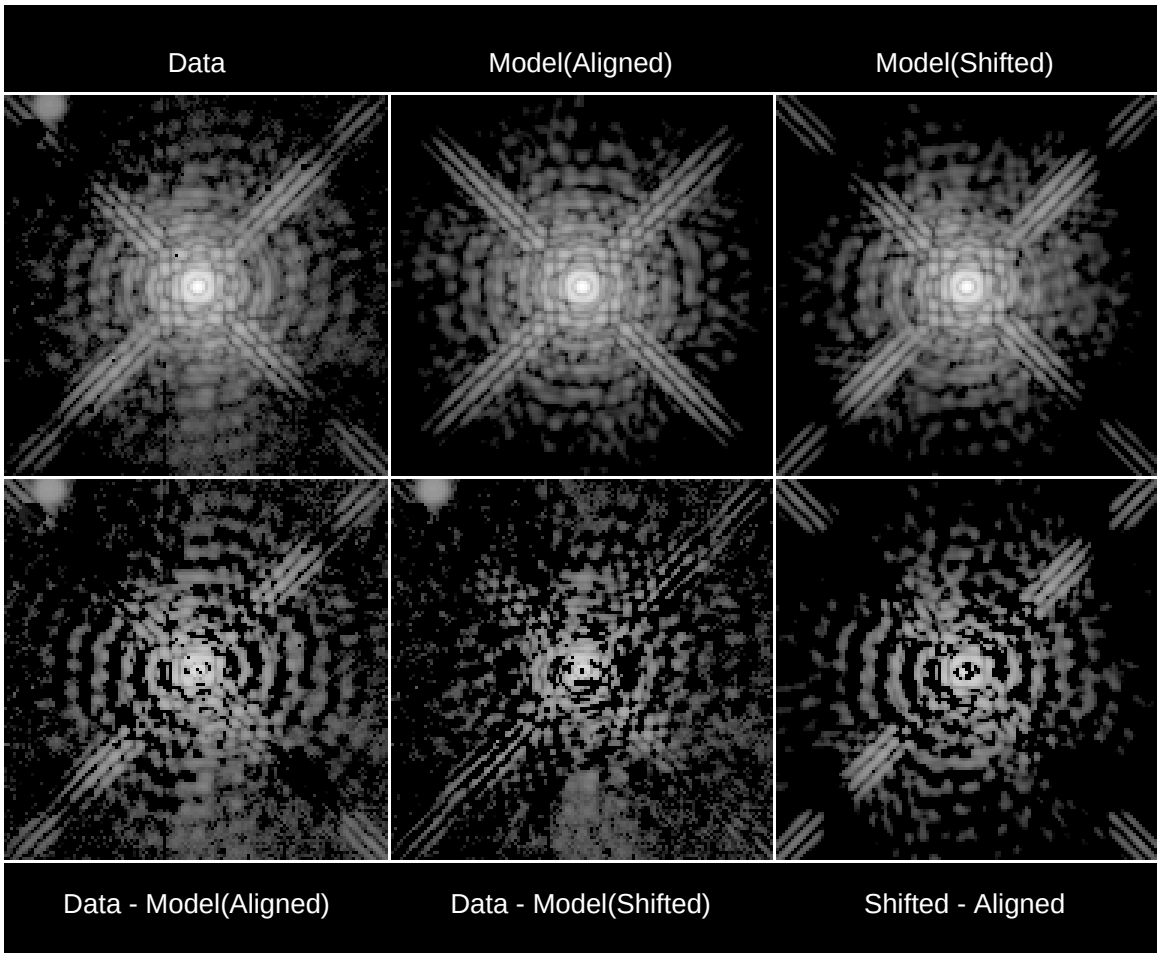

Figure 5. Results of Gerchberg-Saxton phase retrieval on a F222M NICMOS 2 PSF from the SNAP program. On the left is the observed PSF. The retrieved pupil amplitude after one iteration of the algorithm is shown in the middle. Note the elliptical central obscuration. After twenty iterations, the spiders are better defined.

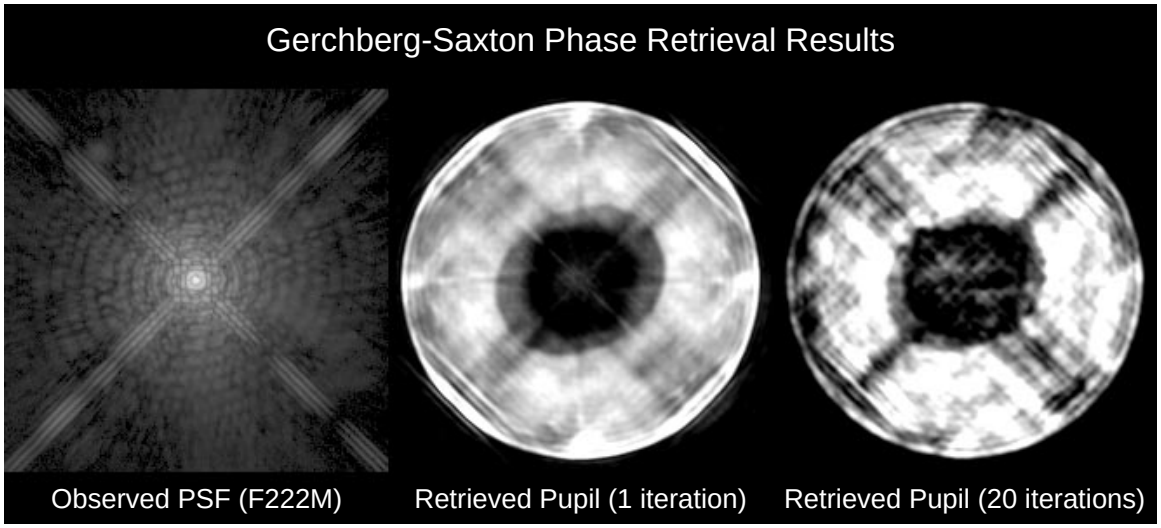

Figure 6. Examples of the effects of time-dependent shifting versus focus changes. The image on the left is the subtraction of one observed NICMOS 2 SNAP PSF from another. The middle panel shows the subtraction of two Tiny Tim model PSFs generated different cold mask shifts. On the right is the difference of two model PSFs, one in-focus and the other with 7μm of breathing. Note the differences in the diffraction spike residuals between the mask shifted and the focus-modified PSFs.

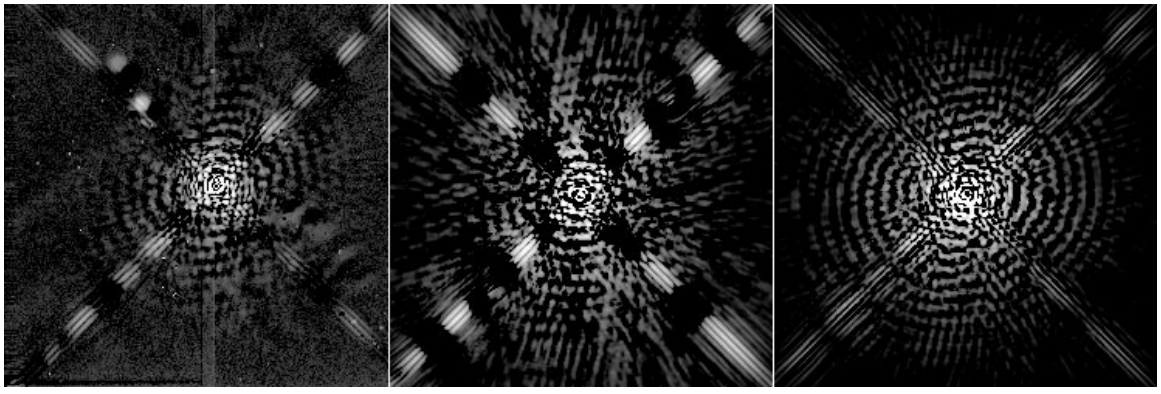

and 7μm by 1.4%. Thus, mask shift in NICMOS 2 is as important as breathing for core photometry, and is more important for PSF subtraction in the wings. The mask shifting affects throughput by less than 0.3%.

Figure 6 shows subtractions using observed PSFs and models with the mask shifted by a small amount (in addition to the large scale shift). The similarity between the two images prove that the residuals seen in the SNAP program subtractions discussed by Krist (1997) are due to time-dependent cold mask shifting.

The diffraction spikes in NICMOS 2 PSFs are 0.5 degrees from being perpendicular, indicating that there is some rotation of the cold mask with respect to the HST obscurations. Because of the added complexity of determining both mask shift and rotation, this effect is not currently included in the Tiny Tim models. It is only obvious in the wings of the PSF (beyond about 4").

NICMOS 1 PSFs show evidence for a similarly shifted mask. NICMOS 3 may also have a shifted mask, but there is currently no known data sufficient to show it.

5. Tiny Tim

Tiny Tim has been used since 1991 to create synthetic HST PSFs for deconvolution, algorithm testing, proposal planning, and optical analysis. It is written in standard C and has been used on a wide variety of computers running VMS, UNIX, and Windows. The software can generate a PSF for a given wavelength or filter passband, and subsampling and jitter are options. Zonal errors in the HST mirrors are included. The PSFs are written out as FITS or GEIS (STSDAS) image files.

Support for NICMOS was added in version 4.2 by Hook with the addition of the cold mask to the pupil pattern and a new option for user-defined spectra/filter throughput tables. Krist added field and focus dependent aberrations to version 4.3 and cold mask misalignment to version 4.4.

The software consists of two programs: `tiny1` and `tiny2`. `Tiny1` asks the user a series of basic questions about the PSF and then generates a parameter file. The second program, `tiny2`, reads the parameter file and computes the PSF model.

The user is asked for the position of the PSF on the detector, the position of the PAM mirror during the observation (provided by the NPFOCUSP keyword in the calibrated data header), and the PAM position for best focus (available on the World Wide Web). The amount of defocus at the center of the field is computed from the difference between PAM positions and then added to the focus value given in the parameter file (which is zero by default but can be changed by the user to investigate breathing effects, etc.). Coma, spherical, and astigmatism are adjusted for focus. Then, the specified PSF position is used to compute the changes to coma, astigmatism, and focus.

Cold mask misalignment is included for NICMOS 1 and 2, while the mask in NICMOS remains aligned. The user can adjust the mask shift by changing values in the parameter file.

Before the addition of NICMOS, the user was allowed to generate either a purely monochromatic PSF or a polychromatic one through a given filter using one of seven object colors. The polychromatic PSF is formed by adding monochromatic PSFs generated at wavelengths sampling the filter's bandpass, with appropriate weighting for filter response and object spectrum. This filter scheme would not have worked as well for NICMOS, given the spectral energy distributions (SEDs) of the objects observed in the infrared. Instead of having to select a combination of a filter and an object color, the user can now provide a list of wavelengths and weights to use for generating a polychromatic PSF. Files containing wavelengths and respective throughputs for NICMOS filters were provided by Glenn Schneider (NICMOS IDT) which a user can multiply by an SED of their choice to provide input to Tiny Tim. This option is available for all cameras, not just NICMOS.

Tiny Tim generates PSFs by computing the Fourier transform of the optical transfer function of a system, which is comprised of the obscuration pattern and wavefront error function. All obscurations are assumed to be in the same plane (thus the coronagraphic mode cannot be modeled using the current code). At each wavelength a critically sampled PSF is generated which is then integrated over detector sized pixels, which may be subsampled if the user wishes.

The NICMOS PSF models produced by Tiny Tim are excellent matches to the observed ones, typically better than those for the other HST cameras. This is due to a number of factors. In the infrared the PSF is less sensitive to aberrations, so mismatches between assumed and actual optical errors are less important than in instruments which observe at shorter wavelengths. Also, because focus runs were obtained on a star cluster, the field and focus- dependent aberrations could be measured for each of the three cameras and incorporated into the models. Unlike WF/PC-1 and WFPC2, the NICMOS obscurations (the cold masks) do not shift with respect to the telescope's depending on position, so the PSF is more stable across the field.

Since a significant portion of the total flux in a NICMOS PSF may be in the diffraction rings or off-center portions of the core (especially in NICMOS 1), there will be some inherent blurring of an object relative to the resolution of the detector. As mentioned previously, such images are candidates for deconvolution, which could improve contrast. Because they are noiseless and easy to obtain, Tiny Tim PSFs are good alternatives to using observed ones.

Acknowledgments. Much of the work described here used NICMOS 2 star images from SNAP program 7420, which are presented with permission of David Golimowski (JHU), Principal Investigator.

References

Krist, J.E., 1997, this volume.

Krist, J.E. & Burrows, C. J., 1995, Appl.Optics, 34, 4951.

Krist, J.E. & Hook, R.N., 1997, *The Tiny Tim User's Manual v4.4* (Baltimore: STScI).